UCRL-11435 Rev.

cy 2

University of California

Ernest O. Lawrence Radiation Laboratory

TWO-WEEK LOAN COPY

This is a Library Circulating Copy which may be borrowed for two weeks. For a personal retention copy, call Tech. Info. Division, Ext. 5545

ANGULAR DISTRIBUTION OF CHARGE-EXCHANGE AND INELASTIC NEUTRONS IN π^--p INTERACTIONS AT 313 AND 371 MeV

Berkeley, California

DISCLAIMER

This document was prepared as an account of work sponsored by the United States Government. While this document is believed to contain correct information, neither the United States Government nor any agency thereof, nor the Regents of the University of California, nor any of their employees, makes any warranty, express or implied, or assumes any legal responsibility for the accuracy, completeness, or usefulness of any information, apparatus, product, or process disclosed, or represents that its use would not infringe privately owned rights. Reference herein to any specific commercial product, process, or service by its trade name, trademark, manufacturer, or otherwise, does not necessarily constitute or imply its endorsement, recommendation, or favoring by the United States Government or any agency thereof, or the Regents of the University of California. The views and opinions of authors expressed herein do not necessarily state or reflect those of the United States Government or any agency thereof or the Regents of the University of California.

UCRL-11435 Rev.

UNIVERSITY OF CALIFORNIA

Lawrence Radiation Laboratory
Berkeley, California

AEC Contract No. W-7405-eng-48

ANGULAR DISTRIBUTION OF CHARGE-EXCHANGE AND INELASTIC NEUTRONS IN π-p INTERACTIONS AT 313 AND 371 MeV

Don L. Lind, Barry C. Barish, Richard J. Kurz,
Philip M. Ogden, and Victor Perez-Mendez

October 26, 1964

ANGULAR DISTRIBUTION OF CHARGE-EXCHANGE AND INELASTIC NEUTRONS IN π-p INTERACTIONS AT 313 AND 371 MeV*

Don L. Lind,† Barry C. Barish,‡ Richard J. Kurz,** Philip M. Ogden,†† and Victor Perez-Mendez

Lawrence Radiation Laboratory
University of California
Berkeley, California

October 26, 1964

ABSTRACT

Neutron angular distributions from the charge-exchange ($\pi^0 n$) and inelastic modes ($\pi^0\pi^0 n$, $\pi^+\pi^- n$) of the $\pi^- p$ interaction have been investigated at 313 and 371 MeV incident-pion kinetic energy. The data were obtained with an electronic counter system. Elastic and inelastic neutrons were separated in the all-neutral final states by time of flight. At both energies the charge-exchange differential cross section at the forward neutron angles differs from that determined by Caris et al. from measurements of the π^0 decay gamma distributions, but generally agrees with the phase-shift analysis calculations of Roper. The distribution of inelastic neutrons from both modes shows a strong preference for low center-of-mass neutron energies. The distribution of these neutrons does not correspond to that expected from the $I=0$, π-π interaction (ABC effect) suggested to account for the anomaly in p-d collisions observed by Abashian et al. Finally, all available charge-exchange differential cross section data from this and other experiments were combined by a least-squares fit to a Legendre expansion of the form

$$\frac{d\sigma}{d\Omega^*} (\cos \theta^* \pi^0) = \sum_{l=0}^{N} a_l P_l (\cos \theta^* \pi^0)$$

with the following results (in mb/sr):

T_{π^-}	a_0	a_1	a_2	a_3
313	1.21±0.03	1.88±0.06	1.61±0.06	0.45±0.06
371	0.89±0.02	1.57±0.04	1.13±0.04	0.38±0.03

I. INTRODUCTION

The angular distribution of final state neutrons occurring in $\pi^- p$ collisions in the 300-400 MeV energy range provides insight into two different aspects of the pion-nucleon interaction. First, the distribution of elastic neutrons (from the reaction $\pi^- p \rightarrow \pi^0 n$) measures directly the differential cross section for this charge-exchange reaction. Secondly, the angular distribution of the inelastic neutrons (from $\pi^- p \rightarrow \pi^0 \pi^0 n$ and $\pi^- p \rightarrow \pi^- \pi^+ n$) provides information about the isotopic state $I = 0$ of the two pions occurring in these inelastic reactions.

At 310 MeV considerable effort has been made to determine an unambiguous phase-shift solution for pion nucleon scattering. Foote et al[1] and Rogers et al.[2] have made a very accurate determination of $\pi^+ p$ differential cross sections and recoil-proton polarization at this energy. Rugge and Vik[3] have provided similarly accurate cross section and polarization data for $\pi^- p$ elastic scattering and have proposed various phase shift solutions which fit all these data.[4]

The inclusion of corresponding data in this phase-shift analysis from the charge-exchange reaction has proven difficult. The only available charge-exchange differential cross section data were those measured by Caris et al.[5] at 317 MeV. However when the Caris data were compared with charge-exchange distributions predicted by phase-shift solutions determined with the elastic-scattering differential-cross-section and polarization data,[4] it was apparent that there was considerable deviation at the backward pion angles.

The charge-exchange distribution had not been measured directly. Because of the extremely short lifetime of the π^0 meson (2.2×10^{-16} sec), only the gamma rays into which it decays could be detected. From this observed

gamma-ray spectrum, the π^0 angular distribution had to be deduced. When the original data analysis was made, the total cross sections for the other final states that contribute to the observed γ rays ($\pi^0\pi^0 n$ and $\pi^-\pi^0 p$) were insufficiently known to provide an accurate correction factor at backward pion angles. It was at these same backward angles that the phase-shift predictions of Vik and Rugge departed most from the charge-exchange data of Caris. In addition, charge-exchange data taken by Kurz[6] at 374 MeV appeared to differ sufficiently from corresponding observations made by Caris to be in significant disagreement. Therefore it was decided to conduct the present experiment to measure the charge-exchange differential cross section by observing the only directly accessible final-state particle—the neutron.

The inelastic neutrons, which we had to identify and separate from the elastic neutron differential cross-section data, occur in association with two-pion final states which contain the isotopic eigenstate $I = 0$. An enhancement of two pion production in this $I = 0$ state has been proposed as an explanation for the anomalous bump in the He^3 momentum spectrum arising from high energy proton-deuterium collisions as observed by Abashian et al.[7,8] (the so-called ABC effect).

If such an enhancement occurs it would alter the distribution of inelastic neutrons. However two groups at Berkeley[6,9] have looked at two-pion final states ($\pi^-\pi^+ n$ and $\pi^0\pi^0 n$) in pion-nucleon collisions and have not observed any clear evidence for such a two-pion interaction. Therefore in the present experiment an analysis of the inelastic neutron distribution was included to provide further information on this question.

Sections II and III discuss briefly the experimental method and data analysis involved in this experiment. This is discussed more completely in reference 10. Section IV presents the results of both the elastic and inelastic neutron measurements. In this last section we also discuss the angular distribution which we derive for the charge-exchange reaction by combining the elastic neutron data from this experiment with the other available data for this reaction.

II. EXPERIMENTAL METHOD

The collision of a negative pion at 313 or 371 MeV laboratory kinetic energy and a proton at rest provides sufficient energy to open some of the inelastic channels of the πN system with the production of an additional final-state pion. Although the higher of these energies is above the threshold for the production of two pions, these contributions are assumed to be negligibly small. Thus we must detect and separate the products of the following reactions.

$\pi^- + p \rightarrow \pi^- + p$	elastic scattering (1)
$\pi^- + p \rightarrow \pi^0 + n$	charge exchange (2)
$\pi^- + p \rightarrow \gamma + n$	radiative absorption (3)
$\pi^- + p \rightarrow \pi^0 + \pi^0 + n$	(4)
$\pi^- + p \rightarrow \pi^- + \pi^+ + n$	pion production (5)
$\pi^- + p \rightarrow \pi^- + \pi^0 + p$	(6)
$\pi^- + p \rightarrow \pi^- + \gamma + p$	nuclear bremsstrahlung (7)

A detector accepting only neutral particles will signal the presence of a neutron (since gamma rays can be distinguished from neutrons, as we show) and will eliminate reactions (1), (6), and (7). The cross section for radiative

absorption (3) is small compared to other neutron sources, so these neutrons can be treated as a mathematical correction to the data. By detecting any charged pions in coincidence with a neutron, reaction (5) can be identified and counted separately. The inelastic neutrons of reaction (4) emerge from the target with a spectrum of energies. At a fixed lab-system angle, the highest of these energies is less than the unique energy of the elastically scattered charge-exchange neutrons (2). This gives a separation between their velocities. Thus the neutrons from reactions (2) and (4) can be separated by their time-of-flight over a measured path length.

The negative pion beam was produced when the internal 732-MeV proton beam of the Berkeley 184-inch synchrocyclotron struck an internal beryllium target 2-in. thick in the beam direction. The pions were deflected outwardly by the magnetic field of the cyclotron. Their trajectory was calculated by the computer program CYCLOTRON ORBITS,[11] which uses measured values of the cyclotron magnetic field to integrate the equations of motion of the particle. A beam transport system consisting of two doublet quadrupole magnets and a momentum-analyzing bending magnet focused the pion beam on the liquid hydrogen target. The current settings of these magnets were determined by the beam optics computer program, OPTIK[12] and by suspended-wire measurements. The angle of deflection in the bending magnet was chosen to produce a recombination at the final image of the momentum dispersion introduced by the cyclotron field. The average energy and energy spread of the beam were experimentally checked by integral range measurements in Cu. The μ^- contamination of the beam due to π^- decays before the bending magnet was determined from these range curves. μ^- production beyond this magnet was calculated and combined with the range-curve information to give the total μ^-

contamination. The electron contamination was estimated from gas Čerenkov counter measurements on similar beams. The properties of the pion beam are listed in Table I.

Figure 1 shows the arrangement of the experimental area beyond the bending magnet M. Located along the pion beam are four scintillation counters (S_1, S_2, S_3, and S_5), which form the beam-monitoring system. Surrounding the hydrogen target is a cylindrical counter (S_4) used to detect charged pions. The four neutron counters (N_{1-4} surrounded by anti-coincidence counters A_{1-4}) are located at representative positions for detecting neutral particles originating in the target.

Counters S_1, S_2, and S_3 were located in the beam to monitor the incident-pion flux arriving at the target position. The smallest counter S_3 defined the area of the beam accepted by the monitor system. S_2 served as the source of the zero-time signal for the time-of-flight analysis. Counter S_5, located beyond the hydrogen target and used in anticoincidence, rejected incident pions that were not scattered by an angle greater than 10 deg in the hydrogen. Counter S_4 detected the presence of one or both of the charged pions in coincidence with a neutron from reaction (5). Thus these "charged mode" neutron events could be recorded separately from the "neutral mode" events [reactions (2) or (4)].

Neutrons were detected in a block of plastic scintillator by observing the light produced by recoiling charged products arising in interactions between the incident neutrons and the hydrogen and carbon nuclei of the scintillator. Gamma rays were similarly registered by the counter, but these could be clearly distinguished by their earlier arrival time. The scintillator block was 4-in. thick in the direction of neutron penetration, and had an octagonal frontal

area formed by removing the corners of a 4X10-in. rectangle. An Amperex 58 AVP phototube with a photocathode 5-1/4 in. in diameter was used in order to obtain efficient light collection from the large block of scintillator.

Each detector was surrounded by an anticoincidence counter which was shaped as an octagonal box completely surrounding the scintillator block and extending back an additional 4 in. beyond the sensitive area. The front face and sides of this counter were formed of 1/4 in. plastic scintillator, and were viewed by two RCA 6810A phototubes whose signals were added. The efficiency of the counter to reject charged particles was estimated as > 99.5%. The four neutron detectors recorded data simultaneously, from positions on both sides of the π^- beam, and at laboratory angles from 10 to 60 deg. The neutron flight path was set at 3, 4, or 5 meters, depending on the angle.

For the time-of-flight analysis the signal from scintillator S_2 was used as the "start" signal for a time-to-height converter. The "stop" signal was generated when a neutral particle registered in one of the neutron detectors. This neutron-timing information was obtained from the phototube signal by pulse differentiation with an overdamped LC-tuned circuit to produce a zero-crossing signal whose zero-crossing point was detected by a tunnel-diode discriminator. This technique was used because the time shift of the output pulse is very small over a large dynamic range of photomultiplier-input light levels.[13] Events were routed according to whether they were "neutral" or "charged" mode and counted in a pulse-height-analyzer (PHA).

Figure 2 shows a PHA record, after all runs for a particular experimental condition had been combined. The yield is shown as a function of PHA channel number which is proportional to the time of flight from the target to the detector. The first particles to arrive are the γ rays, which form the large peak centered at channel 27. These are clearly distinguishable from the

elastic neutrons that arrived next and formed the peak at channel 50. Finally the slower inelastic neutrons are distributed over the next 30 or so channels. Figure 2 was chosen to illustrate the worst situation we encountered in separating the elastic from the inelastic neutrons. At this particular laboratory angle, pion energy, and flight - path distance, the statistical fluctuations due to the low yield leave the least distinguishable "valley" between the two types of neutrons. Still, at this most adverse condition, we were able to unambiguously fit the elastic-neutron peak with a Gaussian curve whose area represents the total-elastic-neutron yield at this angle. Analysis of the gamma peak showed the timing resolution of the entire system to be about 1.5 nsec.

III. DATA ANALYSIS

Before the differential cross sections could be calculated from the neutron yields it was necessary to normalize these yields by the following corrections.

1. Neutron-Detection Efficiency

The neutron-detection efficiency of plastic scintillator is a function of neutron energy, the threshold for the detection of scintillation light, and the detector geometry. A computer program called TOTEFF[14] was used to compute the neutron-detection efficiency as a function of neutron energy for each of the two detection thresholds at which data were taken.

The efficiency varies between 0.07 and 0.17 with an uncertainty of ±10%. This is regarded as an upper limit and it determines the overall uncertainty of the data. The efficiency values obtained from this program are compatible with corresponding measurements made by Wiegand et al.[15]

2. Gamma Conversion

Neutral pion mesons occur as final-state particles in both reactions (2) and (4). If the γ rays into which these mesons decay produce e^+, e^- pairs in the target walls, or if the neutral pion decays in the $\pi^0 \rightarrow \gamma e^- e^+$ mode, and one of the charged particles passes through scintillation counter S_5, the event would be lost. This turns out to be a negligible effect. However if one of the charged particles is detected by S_4, the accompanying neutron would be misconstrued as having arisen from reaction (5). The probability of such a gamma conversion and its subsequent detection was calculated as a function of the laboratory angle of the associated neutron.[10] "Neutral" mode data were increased and "charged" mode data were decreased by this correction.

3. Neutron Rescattering and Absorption

After the initial scattering process in which they are produced, the neutrons can interact with nuclei in the material immediately surrounding the target. This can be either by elastic rescattering, in which case no neutrons would be lost, but the differential distribution of the neutrons might be altered; or the neutrons could interact inelastically with the target nuclei and be absorbed, decreasing the apparent flux at the neutron detectors. The qualitative behavior of rescattering is to shift the elastic-neutron distribution toward the smaller angles where the cross section is lowest. However, even the most adverse assumptions indicated that such a shift would be less than the uncertainty of the neutron-detection-efficiency calculation. In absorption reactions such as $C^{12}(n, \alpha)\ Be^9$ and $Al^{27}(n, p)\ Mg^{27}$, no neutrons exist in the final state. A calculation was made of the decrease in the neutron flux due to these inelastic processes.[10] This attenuation varies as a function of neutron laboratory angle due to the changes

in neutron energy, as well as the varying amount of material encountered when the neutron leaves the target in various directions.

4. Radiative Absorption

Neutrons that originate in the radiative absorption reaction (3) cannot be resolved by time of flight, and must be subtracted from the events recorded in the neutral-mode data. This correction was obtained from a detailed-balance calculation involving the "complementary" reaction, pion photoproduction. The negative pion- photoproduction cross section was obtained from the negative-to-positive pion-photoproduction ratio from deuterium as measured by Neugebauer et al,[16] and the positive-pion-photoproduction cross sections of Walker et al.[17] and Tollestrup et al.[18]

IV. RESULTS

A. Elastic Neutrons

The charge-exchange differential cross sections were computed from the corrected elastic neutron yields and are shown in Figure 3. For comparison with other work these results are plotted as a function of $\theta^*_{\pi^0}$ = c.m. system pion angle = 180° - θ_n^*. (* denotes c.m. system variable.) These results are presented numerically in column (a) of Table II. This data covers the range $21 \leq \theta_n^* \leq 123$ deg. Also shown in Table II are three other classes of data which we have incorporated in an analysis of the angular distribution of reaction (2): column (b) neutron differential cross section at an incident pion kinetic energy T_{π^-} = 374 MeV in the range $84 \leq \theta_n^* \leq 133$ deg,[6] (c) previously published angular distributions at T_{π^-} = 317 and 371 MeV;[5] and (d) the differential cross section at $\theta^*_{\pi^0}$ = 0 deg calculated from forward-direction, fixed-momentum-transfer dispersion relations for pion nucleon scattering.[19] A least-squares analysis was performed to fit these data to the c.m. system differential cross section in the form:

$$\frac{d\sigma}{d\Omega^*}(\cos\theta^*_{\pi^0}) = \sum_{\ell=0}^{N} a_\ell P_\ell(\cos\theta^*_{\pi^0}) . \tag{8}$$

The γ-data were incorporated into the least-squares analysis according to the procedure used by Caris et al.[5] If $d\sigma/d\Omega^*$ is represented as in Eq. (8), the expected experimental γ-angular distribution in the c.m. system, taking into the account the γ detection efficiency of the experimental system, is given by

$$\frac{d\sigma^{\gamma}}{d\Omega^{*}}(\cos\theta_{\gamma}^{*}) = \sum_{\ell=0}^{N} a_{\ell} P_{\ell}(\cos\theta_{\gamma}^{*}) \int_{-1}^{1} \frac{dx P_{\ell}(x)\epsilon(k)}{(\gamma-\eta x)^{2}} , \tag{9}$$

where x is the cosine of the angle between the photon and the π^0 in the c.m. system, γ and η denote the motion of the π^0 rest system with respect to the c.m. system, and $\epsilon(k)$ is the γ-detector efficiency as a function of the photon lab-system energy, k, which in turn is a function of x and $\cos\theta_{\gamma}^{*}$.

The present analysis started with the uncorrected data of Caris et al. (see Table IV, Ref. 5). The correction of the observed distributions to take into account photons originating from the reactions $\pi^- p \rightarrow \pi^0\pi^0 n$ and $\pi^-\pi^0 p$ was reperformed. The availability of more precise information on these reactions made a more accurate estimation of the correction feasible.[20] For each reaction we assume that the π^0's had an invariant phase-space energy distribution and an isotropic angular distribution in the c.m. system. We calculated the corresponding lab-system distribution of photons in energy and angle, $d^2\sigma/dkd\Omega$, with a normalization determined by the total cross sections for the $\pi^0\pi^0 n$ and $\pi^-\pi^0 p$ reactions. To obtain the values of $d\sigma^{\gamma}/d\Omega^{*}$ used in this analysis, we subtracted the quantity,

$$\frac{d\sigma^{inel}}{d\Omega}(\theta_{\gamma}) = \int dk \frac{d^2\sigma(k,\theta_{\gamma})}{dkd\Omega}\epsilon(k) , \tag{10}$$

from the uncorrected data points of Caris et al. We used their original values for the remaining corrections that they discuss. The values used in the least-squares analysis are given in Table II column (c).

The neutron data provided information on the portion of the angular distribution in which the uncertainties in the γ data are greatest. The relative magnitude of the calculated corrections to the γ-angular distribution is greater

for $\theta^*_\gamma > 90$ deg. In addition, the statistical weight of the γ data is lowest in this region.

We performed the least-squares analysis with (a) the recorrected γ data alone, (b) the neutron data and the dispersion-relation points, and (c) all data simultaneously. The results are given in Table III. At $T_{\pi^-} = 315$ (the average T_{π^-} for the various data) and 371 MeV the probability of fit was not significantly increased for $N > 2$ for case (a) and for $N > 3$ for cases (b) and (c). At $T_{\pi^-} = 315$ MeV for case (c) the γ-data point at $\cos\theta^*_\gamma = -0.955$ was deleted since the inclusion of this point decreased the probability of fit to 0.001.

The differential cross section for $\pi^- p \rightarrow \pi^0 n$ at $T_{\pi^-} = 315$ and 371 MeV as determined by the least-squares analysis of the recorrected γ data and by the analysis of the combined data are plotted in Figure 4. The non-zero value of a_3 obtained in the combined data analysis is consistent with the requirement of at least D-waves in other analyses of pion-nucleon interactions at $T_{\pi^\pm} = 310$ MeV.[4] However, the behavior of the angular distribution in the region of $\theta^*_{\pi^0} = 180$ deg is not consistent with any of the SPD-solutions of Vik and Rugge. The same comment applies to the results of measurements of the neutron polarization in $\pi^- p \rightarrow \pi^0 n$ at $T_{\pi^-} = 310$ MeV.[21] The differential cross section obtained here corresponds most closely to predictions obtained from SPDF-solutions II and IV of Vik and Rugge.[22] We note that the SPDF-solution II of Vik and Rugge is preferred by the recent theoretical analysis of pion-nucleon scattering of Donnachie et al.[23] The angular distribution at $T_{\pi^-} = 315$ and 371 MeV presented here deviates from that determined from the

γ data alone in a manner which is in agreement with the predictions of an energy-dependent phase-shift analysis of pion-nucleon scattering by Roper.[22, 24] The predictions by Roper at $T_{\pi^-} = 310$ and 370 MeV are also plotted in Figure 4. He used the data of Caris et al. in his analysis as well as all other available data on pion-nucleon scattering (including the neutron polarization data referred to above). At both energies, $d\sigma/d\Omega^*$ for $\theta^*_{\pi^0} < 90$ deg is lower than the predictions by Roper. At $\theta^*_{\pi^0} = 180$ deg, isotopic spin considerations place a lower limit on $d\sigma/d\Omega$ for $\pi^- p \rightarrow \pi^0 n$ in terms of the differential cross sections for $\pi^\pm p \rightarrow \pi^\pm p$ at $\theta_\pi = 180$ deg.

$$\frac{d\sigma^0}{d\Omega} \geq \frac{1}{2} \left[\left(\frac{d\sigma^+}{d\Omega}\right)^{1/2} - \left(\frac{d\sigma^-}{d\Omega}\right)^{1/2} \right]^2 \tag{11}$$

If we use the available data on elastic scattering,[2, 3, 25] this limit is 0.77 ± 0.20 mb/sr at $T_{\pi^-} = 310$ MeV and 0.13 ± 0.06 mb/sr at $T_{\pi^-} = 370$ MeV. The values corresponding to the N = 3, combined-data of Table III are 0.50 ± 0.11 mb/sr and $0.07 \pm$ mb/sr respectively. Thus the present charge-exchange angular distributions $\theta^*_{\pi^0} = 180$ deg are barely compatible with this limit.

By integration of the $d\Omega^*$ curve over $\cos\theta^*_{\pi^0}$, a value for the total cross section σ_T for the reaction (2) was obtained. These results are presented in Table IV and are calculated from the "combined" data Table III with N = 3.

B. Inelastic Neutrons

The inelastic-neutron distributions can be compared to phase-space distributions and distributions enhanced by an $I=0$ two-pion interaction, in either of two ways. The first is at a constant neutron angle. This would correspond to a vertical cut through the kinematically allowed inelastic area shown in Figure 5. In effect, this is what is shown in the inelastic distribution in Figure 2 except that the abscissa has been plotted as time-of-flight instead of neutron energy. The second possibility is at a constant neutron energy. This corresponds to a horizontal cut through the inelastic neutrons areas in Figure 5. In this case an energy band can be selected sufficiently wide to avoid the statistical fluctuations seen in Figure 2. In addition, since the neutron energy is constant, any inaccuracy in the neutron-detection efficiency is eliminated from the shape of the distribution. A calculation of the second type gives $d^2\sigma/dt\ d\Omega$ for constant T_N for both $\pi^+\pi^-n$ and $\pi^0\pi^0n$ final states; this is presented numerically in Table V and graphically in Figures 6 and 7. Also shown in the figures are the phase-space distribution and the distribution calculated by using an $I=0$ two-pion interaction enhancement factor with $a_0 = 2\mu^{-1}$ and $R=0$. This value of a_0 is the scattering length tentatively proposed by Abashian et al.[8] for the $I=0$ two-pion interaction, and $R=0$ is the radius of interaction. These curves are normalized to the integral of the distribution for $\pi^+\pi^-n$ over $\cos\theta$.

The distribution of inelastic neutrons from the $\pi^+\pi^-n$ final state departs noticeably from both the phase-space distribution and the ABC enhancement distribution. We observe that there is a strong peaking at low c.m. energy for the neutron. This same effect was observed by Kirz et al.,[9] Barish et al.,[20] and Blokhintseva et al.[26] These low-neutron energies correspond to a dipion effective mass in the range (near $m_{\pi\pi} = 400$ MeV) where several authors report

I = 0 two-pion resonances.[27-29] This low-energy peaking seems to be present at $T_{\pi^-} = 371$ MeV in the $\pi^0\pi^0 n$ distribution, which is in agreement with Barish et al. but is not clearly evident at 313 MeV. However, at this energy the large statistical errors of the data do not justify any firm conclusions.

The enhancement of the distribution from an I = 0 two-pion interaction, which has been proposed to explain the anomaly observed by Abashian et al.[8] is not observed. However the domination of the distribution by a strong enhancement at the opposite end of the neutron-c.m.-energy range may mask this effect. Finally we note that an explanation has been proposed by Anisovich and Dakhno for both of these enhancements in terms of a singularity in the scattering amplitude.[30]

ACKNOWLEDGMENTS

We would like to acknowledge the help, support and encouragement received from Professor Burton J. Moyer thoughout the course of this experiment. We are indebted to Dr. Julius Solomon for his assistance in the beam-optics calculations and to Dr. L. David Roper for his helpful discussions and cooperation in transmitting the results of his phase-shift analysis. We are grateful to Dr. T. D. Spearman for pointing out the limit on charge-exchange differential cross sections at 180 deg. Finally we would like to thank James T. Vale and the members of the cyclotron crew for their help and cooperation during this experiment.

FOOTNOTES AND REFERENCES

*Work done under the auspices of the U.S. Atomic Energy Commission.

†Present address: Goddard Space Flight Center, Greenbelt, Maryland.

‡Present address: Synchrotron Laboratory, California Institute of Technology, Pasadena, California.

**Present address: Ecole Polytechnique, Paris, France.

††Present address: Seattle Pacific College, Seattle, Washington.

1. J. Foote, O. Chamberlain, E. Rogers, H. Steiner, C. Wiegand and T. Ypsilantis, Phys. Rev. 122, 948 (1961).
2. E.H. Rogers, O. Chamberlain, J. Foote, H. Steiner, C. Wiegand, and T. Ypsilantis, Rev. Mod. Phys. 33, 356 (1961).
3. Hugo R. Rugge and Olav T. Vik, Phys. Rev. 129, 2300 (1963).
4. Olav T. Vik, and Hugo R. Rugge, Phys. Rev. 129, 2311 (1963).
5. J.C. Caris, R.W. Kenney, V. Perez-Mendez, and W.A. Perkins, Phys. Rev. 121, 893 (1961).
6. Richard J. Kurz, Differential Distributions of Neutrons in Inelastic $\pi^- p$ interactions at 374, 417, and 454 MeV (Ph.D. Thesis), UCRL-10564, Nov. 1962.
7. Alexander Abashian, Norman E. Booth, and Kenneth M. Crowe, Phys. Rev. Letters 5, 258 (1960); Norman E. Booth, Alexander Abashian, and Kenneth M. Crowe, Phys. Rev. Letters 7, 35 (1961).
8. Alexander Abashian, Norman E. Booth, Kenneth M. Crowe, Roger E. Hill, and Ernest H. Rogers, Phys. Rev. 132, 2296; 2305; 2309; 2314 (1963).
9. Janos Kirz, Joseph Schwartz, and Robert D. Tripp, Phys. Rev. 130, 2481 (1963).

10. Don L. Lind, Differential Distribution of Charge-Exchange and Inelastic Neutrons in π^--p Interactions at 313 and 371 MeV (Ph. D. Thesis) UCRL-11435, July 1964.

11. Joe Good, Morris Pripstein, and Howard S. Goldberg, CYCLOTRON ORBITS: A 709 Ray-Trace Program for Cylindrically Symmetric Magnetic Fields, UCRL-11044, Oct. 1963.

12. Thomas J. Devlin, OPTIK: An IBM 709 Computer Program for the Optics of High-Energy Particle Beams, UCRL-9727 Sept. 1961.

13. Arthur E. Bjerke, Quentin A. Kerns, and Thomas A. Nunamaker, Pulse Shaping and Standardizing of Photomultiplier Signals for Optimum Timing Information Using Tunnel Dioides, UCRL-9838, Aug. 1961.

14. Richard J. Kurz, A 709/7090 Fortran II Program to Compute the Neutron-Detection Efficiency of Plastic Scintillator for Neutron Energies from 1 to 300 MeV, UCRL-11339, March 1964.

15. Clyde E. Wiegand, Tom Elioff, William B. Johnson, Leonard B. Auerbach, Joseph Lach, and Thomas Ypsilantis, Detection Efficiency of Plastic Scintillator for Neutron Energies 4 to 76 MeV, UCRL-9986, Dec. 1961.

16. Gerry Neugebauer, Walter Wales, and R. L. Walker, Phys. Rev. 119, 1726 (1960).

17. R. L. Walker, J. G. Teasdale, V. Z. Peterson, and J. A. Vette, Phys. Rev. 99, 210 (1955).

18. A. V. Tollestrup, J. C. Keck, and R. M. Worlock, Phys. Rev. 99, 220 (1955).

19. David Cheng (Lawrence Radiation Laboratory, Berkeley), private communication, 1964.

20. Barry C. Barish, Richard J. Kurz, Victor Perez-Mendez, and Julius Solomon, Inelastic π^--p Interactions in the Energy Range of 310 to 454 MeV, Phys. Rev. 135, B416 (1964).

21. Roger E. Hill, Norman E. Booth, Robert J. Esterling, David L. Jenkins, Norman H. Lipman, Hugo R. Rugge, and Olav T. Vik, Bull. Am. Phys. Soc. 9, 410 (1964).

22. L. David Roper (Lawrence Radiation Laboratory, Livermore) private communication, 1964.

23. A. Donnachie, J. Hamilton, and A. T. Lea, Prediction of p-, d-, and f-Wave Pion-Nucleon Scattering, Phys. Rev. 135, B515 (1964).

24. L. David Roper, Phys. Rev. Letters 12, 340 (1964).

25. Phillip M. Ogden, Donald E. Hagge, Jerome A. Helland, Marcel Banner, Jean Francois Detoeuf, and Jacques Teiger, (UCRL-11180, Rev., June 1964) submitted to Phys. Rev.

26. T. D. Blokhintseva, V. G. Grebinnik, V. A. Zhukov, G. Libman, L. L. Nemenov, G. I. Selivanov, and Y. Jung-Fang, Soviet Physics--JETP (English Transl.) 17, 80 (1963).

27. N. P. Samios, A. H. Backman, R. M. Lea, T. E. Kalogerpoulos, and W. D. Shepard, Phys. Rev. Letters 9, 139 (1962).

28. R. Del Fabbra, M. DePretis, R. Jones, G. Marini, A. Odian, G. Stoppini, and L. Tau, Phys. Rev. Letters 12, 674 (1964).

29. C. Richardson, R. Kraemer, M. Meer, N. Nussbaum, A. Pevsner, R. Strand, T. Toohig and M. Block, Two-Pion Resonances Below Mass 900 MeV, in Proceedings of the International Conference on High-Energy Nuclear Physics, Geneva, 1962, I. Prentki, Ed. (CERN, Scientific Information Service, Geneva, Switzerland, 1962), p. 96.

30. V. V. Anisovich and L. G. Dakhno, Phys. Rev. Letters 10, 221 (1964).

Table I. Summary of π^- beam characteristics.

Energy (MeV)	ΔT (MeV)	Intensity (π/min)	Muon contamination (%)	Electron contamination (%)
313	14	25×10^6	5.8	0.3
371	13	12×10^6	4.0	0.3

Table II. $\pi^- p \to \pi^0 n$ angular distribution data for various values (in MeV) of T_{π^-} (a, b, c, and d refer to the designations in Section IV of the text).

a		b		c		d	
$\cos\theta^*_n$	$d\sigma/d\Omega^*$ (mb/sr)	$\cos\theta^*_n$	$d\sigma/d\Omega^*$ (mb/sr)	$\cos\theta^*_\gamma$	$d\sigma^\gamma/d\Omega^*$ (mb/sr)	$\cos\theta^*_{\pi^0}$	$d\sigma/d\Omega^*$ (mb/sr)
313 MeV				317 MeV		315 MeV	
-0.536	1.77±0.20			1.000	2.80±0.20	1.000	4.30±0.57
-0.385	1.40±0.14			0.889	2.44±0.15		
-0.222	0.73±0.07			0.779	2.18±0.14		
-0.050	0.44±0.04			0.598	1.64±0.11		
0.125	0.27±0.03			0.225	0.80±0.06		
0.297	0.23±0.02			-0.199	0.29±0.05		
0.461	0.27±0.03			-0.589	0.21±0.04		
0.612	0.32±0.04			-0.869	0.39±0.04		
0.745	0.37±0.04			-0.952	0.31±0.05		
0.853	0.41±0.05						
0.933	0.46±0.10						
371 MeV		374 MeV		371 MeV		371 MeV	
		-0.678	1.69±0.17	1.000	2.59±0.17	1.000	3.65±0.65
-0.545	1.59±0.16	-0.545	1.31±0.13	0.970	2.25±0.15		
		-0.400	0.97±0.10	0.882	2.12±0.13		
-0.233	0.60±0.06	-0.233	0.62±0.06	0.766	1.84±0.11		
		-0.062	0.41±0.04	0.577	1.23±0.08		
0.113	0.22±0.02			0.194	0.60±0.05		
0.500	0.14±0.01			-0.230	0.23±0.04		
0.740	0.11±0.01			-0.610	0.14±0.05		
0.932	0.10±0.01			-0.877	0.05±0.05		
				-0.955	0.26±0.05		

Table III. Results of the least-squares fits of the differential cross section for $\pi^- p \rightarrow \pi^0 n$ to the form

$$\frac{d\sigma}{d\Omega^*}(\cos\theta^*_{\pi^0}) = \sum_{\ell=0}^{N} a_\ell P_\ell(\cos\theta^*_{\pi^0}).$$

T_{π^-} (MeV)		N	a_0	a_1	a_2	a_3	Probability of fit
			(mb/sr)				
315	a	2	1.31±0.04	1.86±0.08	1.57±0.11	-	0.57
	b	2	0.92±0.04	1.17±0.08	0.96±0.07	-	10^{-3}
		3	1.13±0.06	1.73±0.14	1.50±0.13	0.44±0.09	0.88
	c	2	1.16±0.03	1.62±0.05	1.31±0.05	-	$< 10^{-4}$
		3	1.21±0.03	1.88±0.06	1.61±0.06	0.45±0.06	0.40
371	a	2	1.00±0.03	1.62±0.06	1.12±0.08	-	0.15
	b	2	0.60±0.02	0.89±0.05	0.44±0.03	-	$< 10^{-4}$
		3	0.80±0.03	1.37±0.08	0.96±0.07	0.31±0.04	0.75
	c	2	0.77±0.02	1.26±0.03	0.67±0.02	-	$< 10^{-4}$
		3	0.89±0.02	1.57±0.04	1.13±0.04	0.38±0.03	0.12

a. γ data only.

b. Neutron data and forward direction dispersion relation point.

c. All data combined.

Table IV. Total charge-exchange cross section

T_{π^-} (MeV)	σ_T (mb)
313	15.1±0.4
371	11.1±0.2

Table V. Inelastic neutron $d^2\sigma/dT\ d\Omega$ distribution at constant neutron energy.

T_{π^-} (MeV)	Cos θ_n	$d^2\sigma/dT\ d\Omega(\pi^+\pi^-n)$ (μb/MeV-sr)	$d^2\sigma/dT\ d\Omega(\pi^0\pi^0n)$ (μb/MeV-sr)
313	0.985	57.3±16.8	
	0.966		10.9±16.5
	0.959	33.5±6.2	
	0.940		12.7±13.9
	0.906	16.0±8.8	8.3±14.0
	0.866	11.7±2.7	7.9± 3.9
	0.819	7.1±2.7	3.6± 4.0
	0.766	6.7±2.6	5.9± 4.3
371	0.985	60.1±11.0	18.7±10.7
	0.940	36.4± 5.5	20.0± 7.0
	0.866	15.2± 3.9	8.9± 4.4
	0.766	6.0± 2.8	0.4± 4.2

FIGURE CAPTIONS

Figure 1. Plan view of the experimental area showing target and counter arrangement.

Figure 2. Neutral-mode time-of-flight spectra. The solid line histogram is the neutral-particle yield. The dashed line is a Gaussian curve fitted to the elastic-neutron peak. (The detailed structure of the spectra is discussed in the text).

Figure 3. Charge-exchange differential cross section at $T_{\pi^-} = 313$ and 371 MeV.

- □ Measured in this experiment (313 MeV)
- ○ Measured in this experiment (371 MeV)
- ● Measured by Kurz (374 MeV)
- △ Forward-dispersion-relation calculation

Curves are least-squares fits to the data.

Figure 4. Comparison of differential cross section data.

——— combined neutron and gamma data

—·—· gamma data only

— — — differential cross section predicted by Roper phase-shift solutions.

Figure 5. Laboratory-system neutron kinematics for the processes $\pi^- p \rightarrow \pi \pi n$ (region inside curve A) and $\pi^- p \rightarrow \pi^0 n$ (curve B) at 313 MeV. Curves at 371 MeV are similar. Shaded area is energy band used in inelastic neutron analysis.

Figure 6. Inelastic-neutron differential distribution for $T_{\pi^-} = 313$ MeV (neutron energy interval from 42 to 57 MeV).

○ $d^2\sigma/dtd\Omega$ for $\pi^+\pi^-n$

● $d^2\sigma/dtd\Omega$ for $\pi^0\pi^0n$

A phase-space distribution

B distribution for $I = 0$ two-pion interaction with $a_0 = 2\mu^{-1}$ and $R = 0$.

Figure 7. Inelastic-neutron differential distribution for $T_{\pi^-} = 371$ MeV (neutron energy interval from 50 to 69 MeV).

○ $d^2\sigma/dtd\Omega$ for $\pi^+\pi^-n$

● $d^2\sigma/dtd\Omega$ for $\pi^0\pi^0n$

A phase-space distribution

B distribution for $I = 0$ two-pion interaction with $a_0 = 2\mu^{-1}$ and $R = 0$.

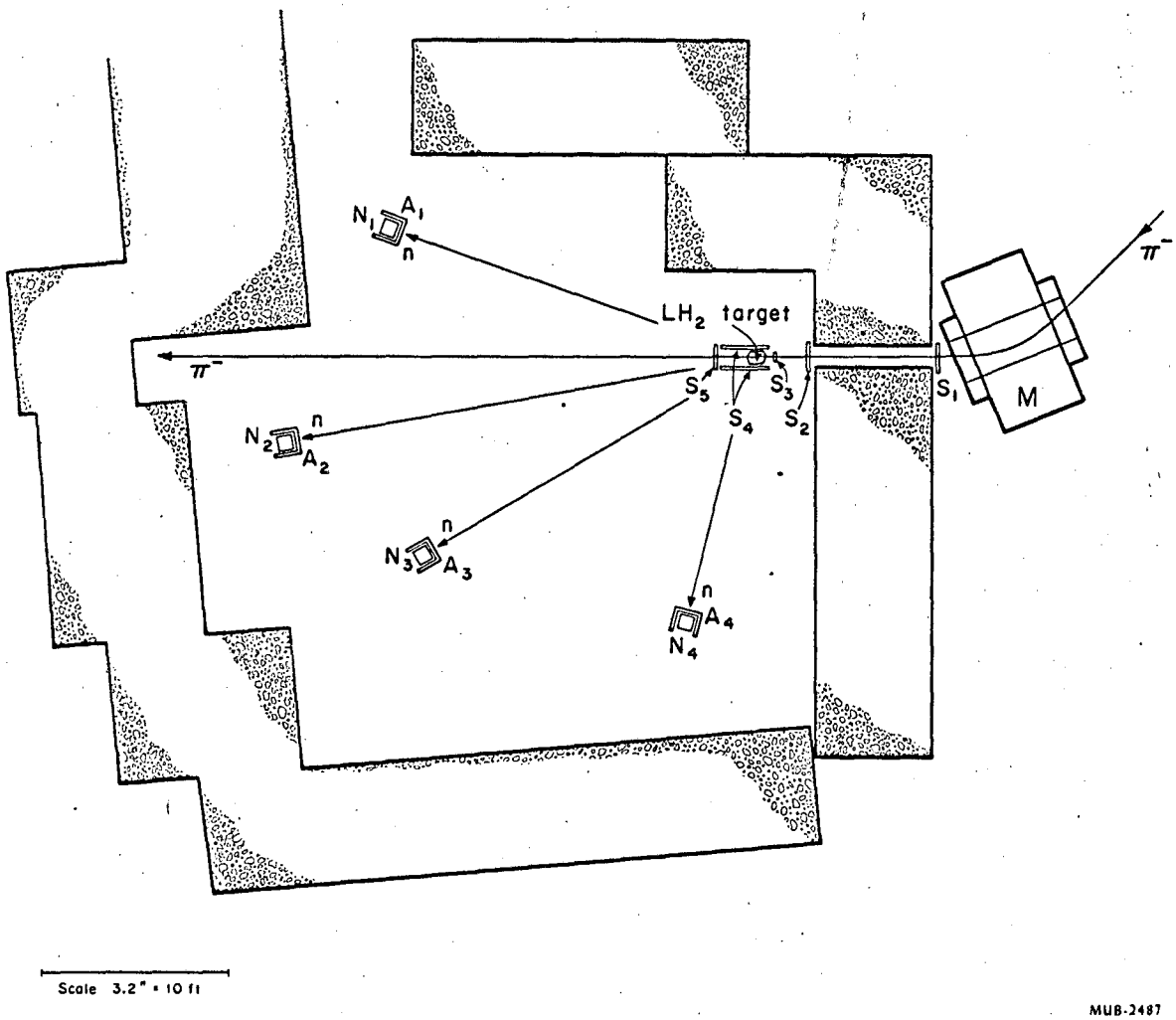
N1
A1
n
LH2 target
π⁻
π⁻
S5
S3
S4
S2
S1
M
N2
n
A2
N3
n
A3
n
A4
N4
Scale 3.2" = 10 ft
MUB-2487

Fig. 1

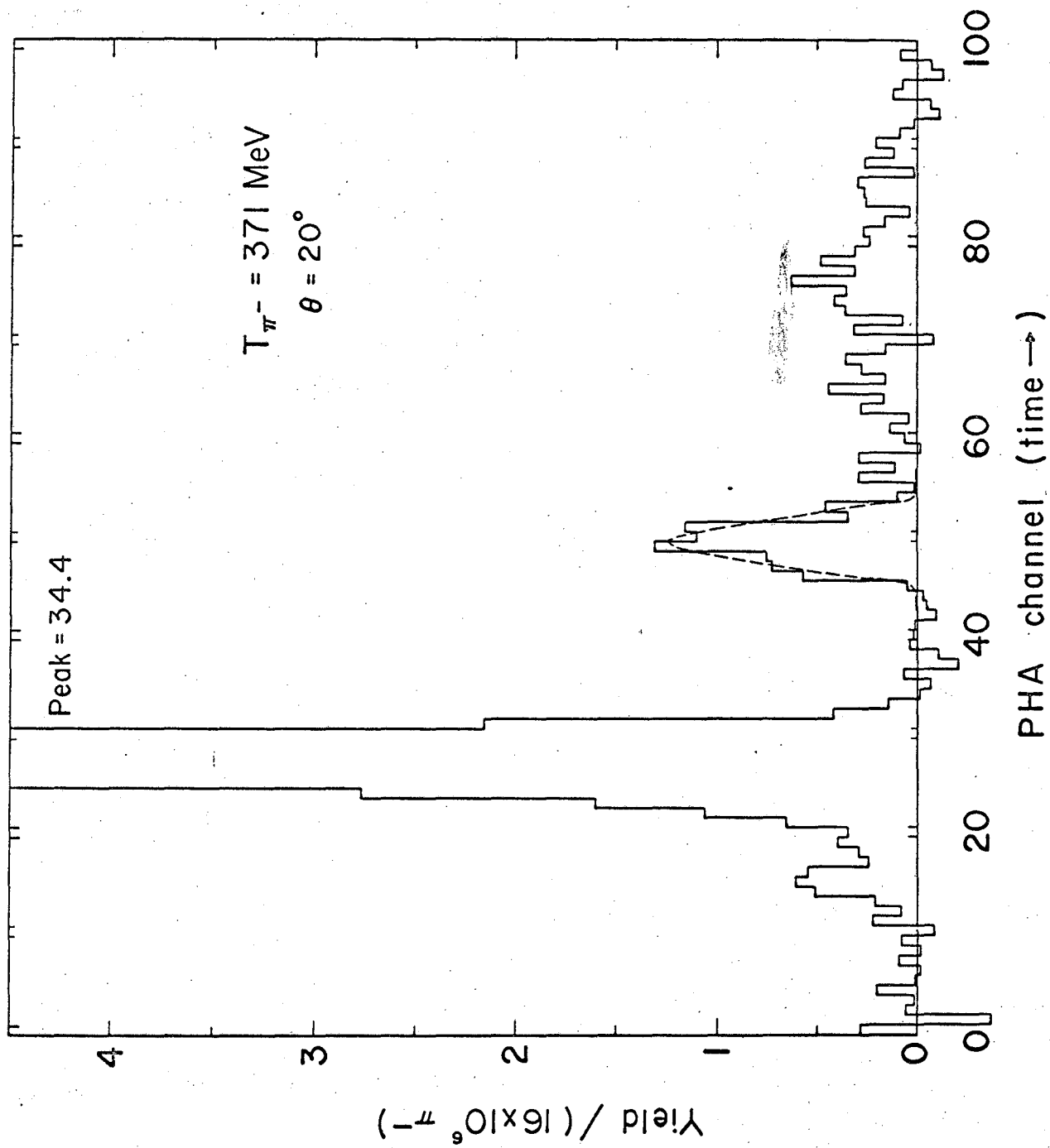

MUB-2489

Fig. 2

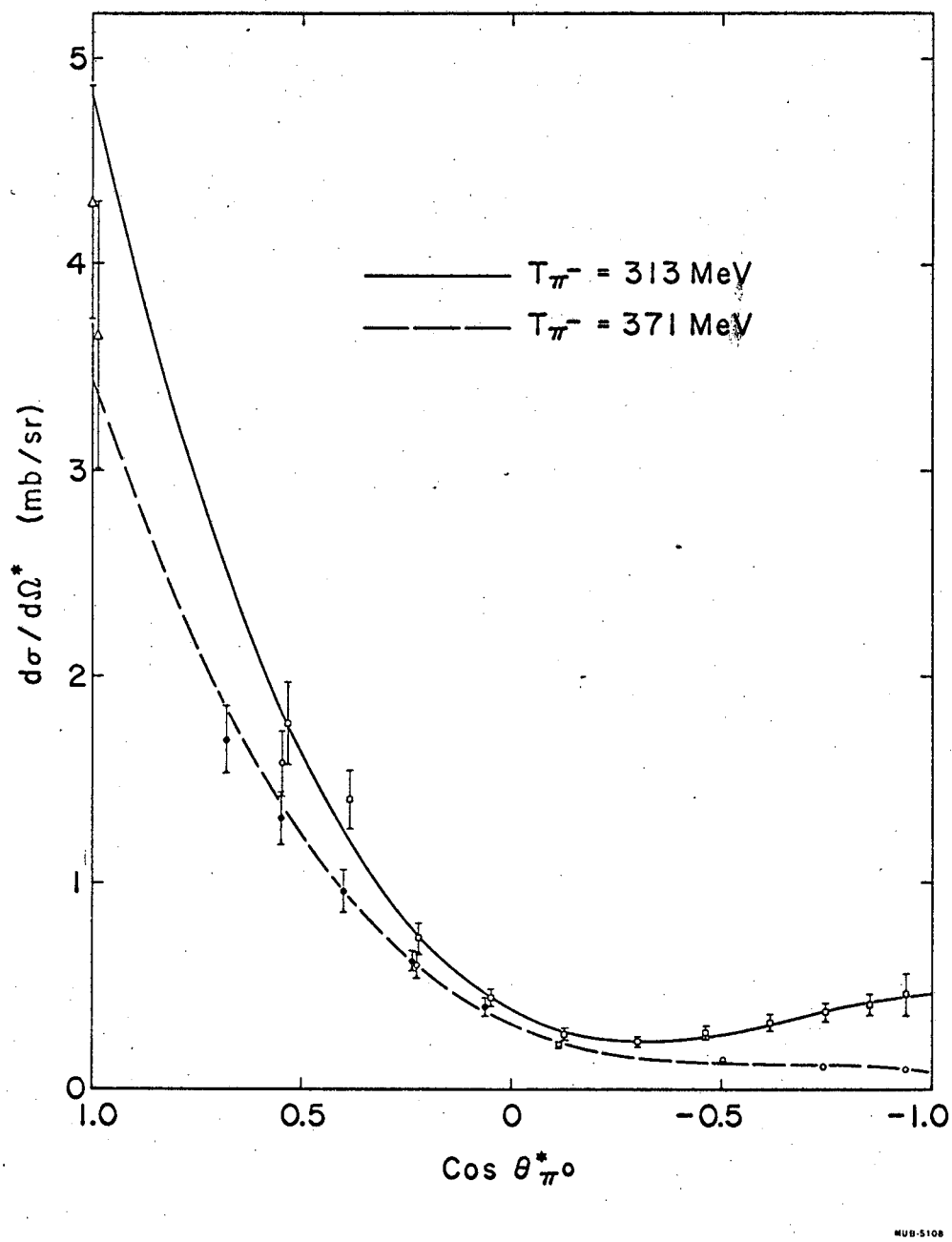
5
4
3
2
1
0
1.0
0.5
0
-0.5
-1.0
$d\sigma/d\Omega^*$ (mb/sr)
Cos $\theta^*_{\pi^0}$
T_{π^-} = 313 MeV
T_{π^-} = 371 MeV
MUB-5108

Fig. 3

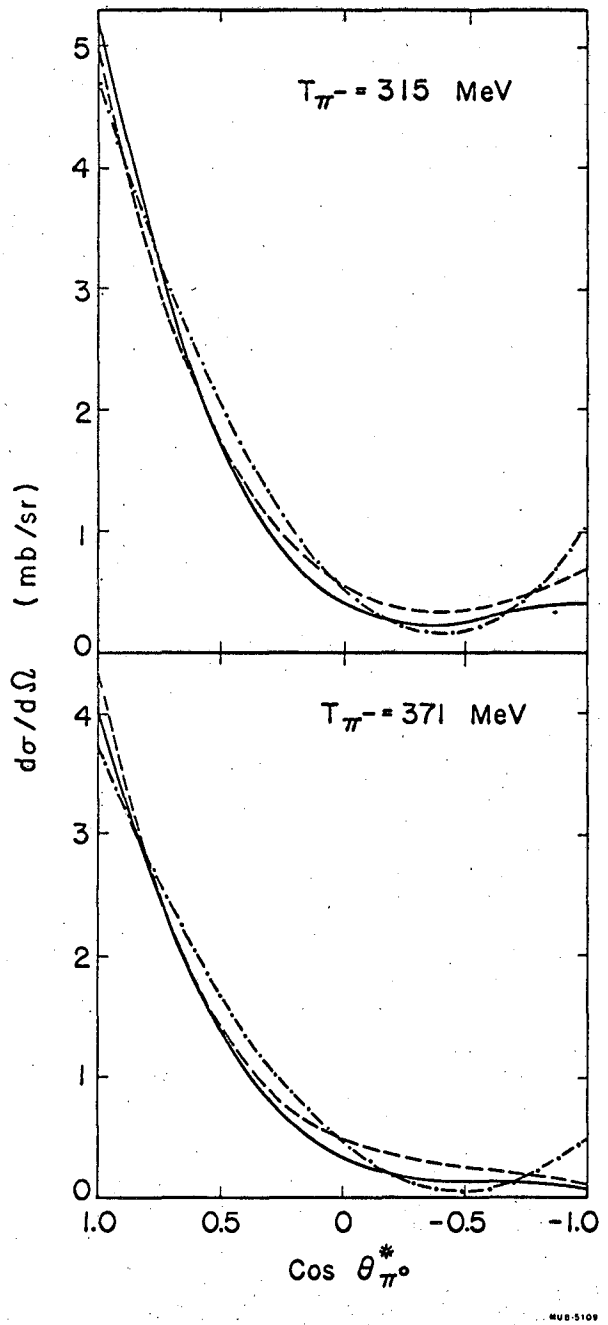
T_{π^-} = 315 MeV
T_{π^-} = 371 MeV
$d\sigma/d\Omega$ (mb/sr)
Cos $\theta^*_{\pi^0}$
1.0
0.5
0
-0.5
-1.0
0
1
2
3
4
5
MUB-5109

Fig. 4

313 MeV

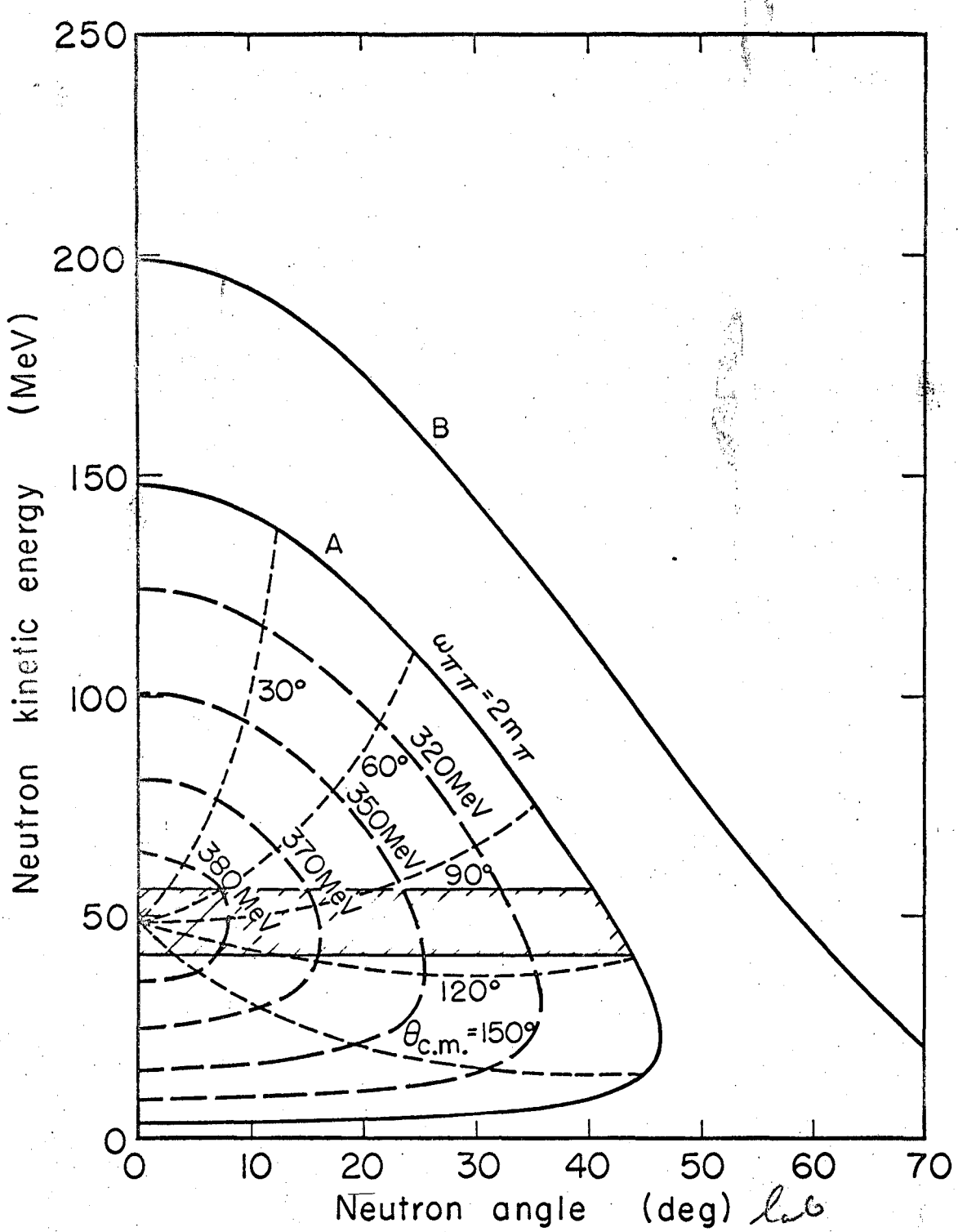

MU-34128

Fig. 5

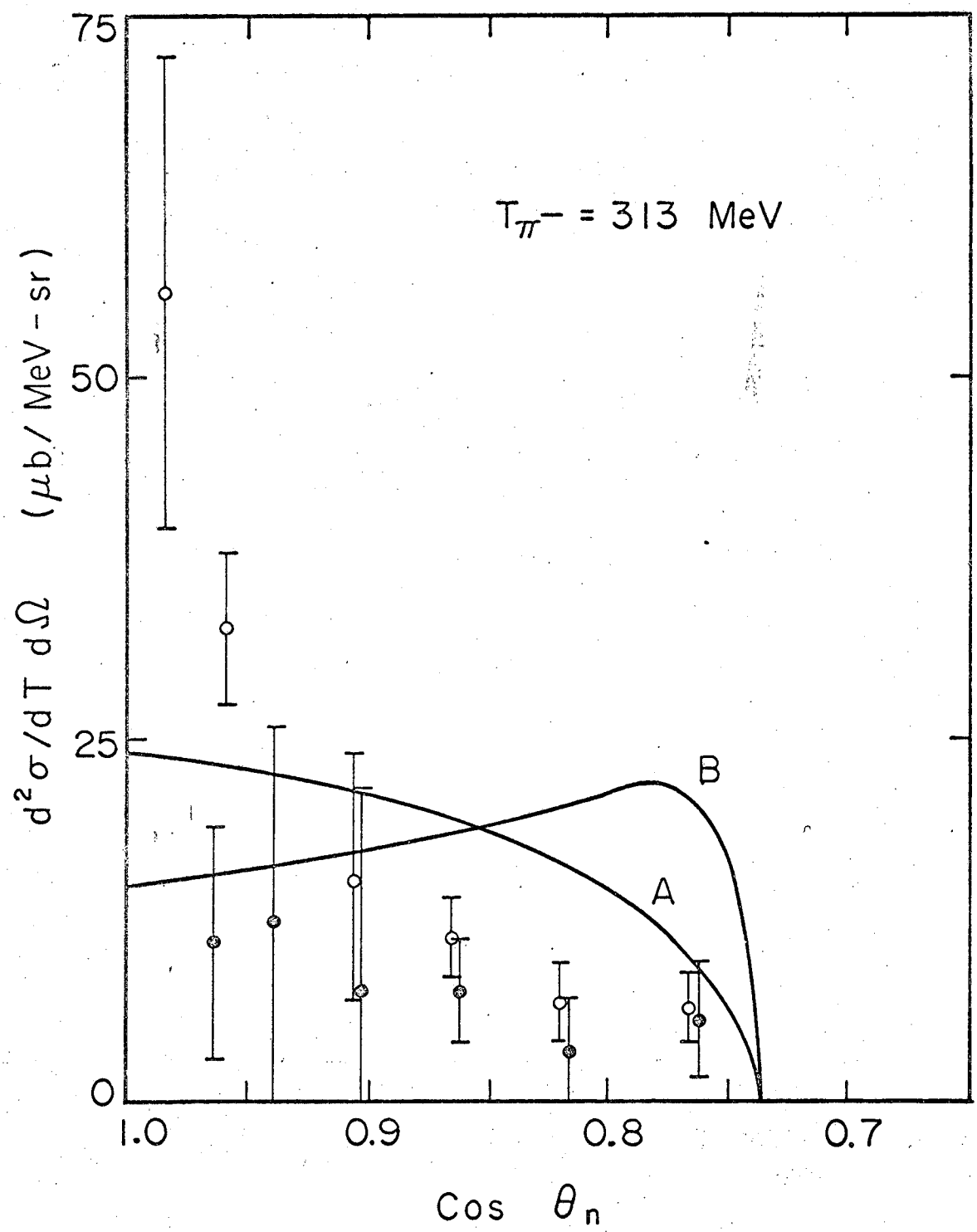

MU-34130

Fig. 6

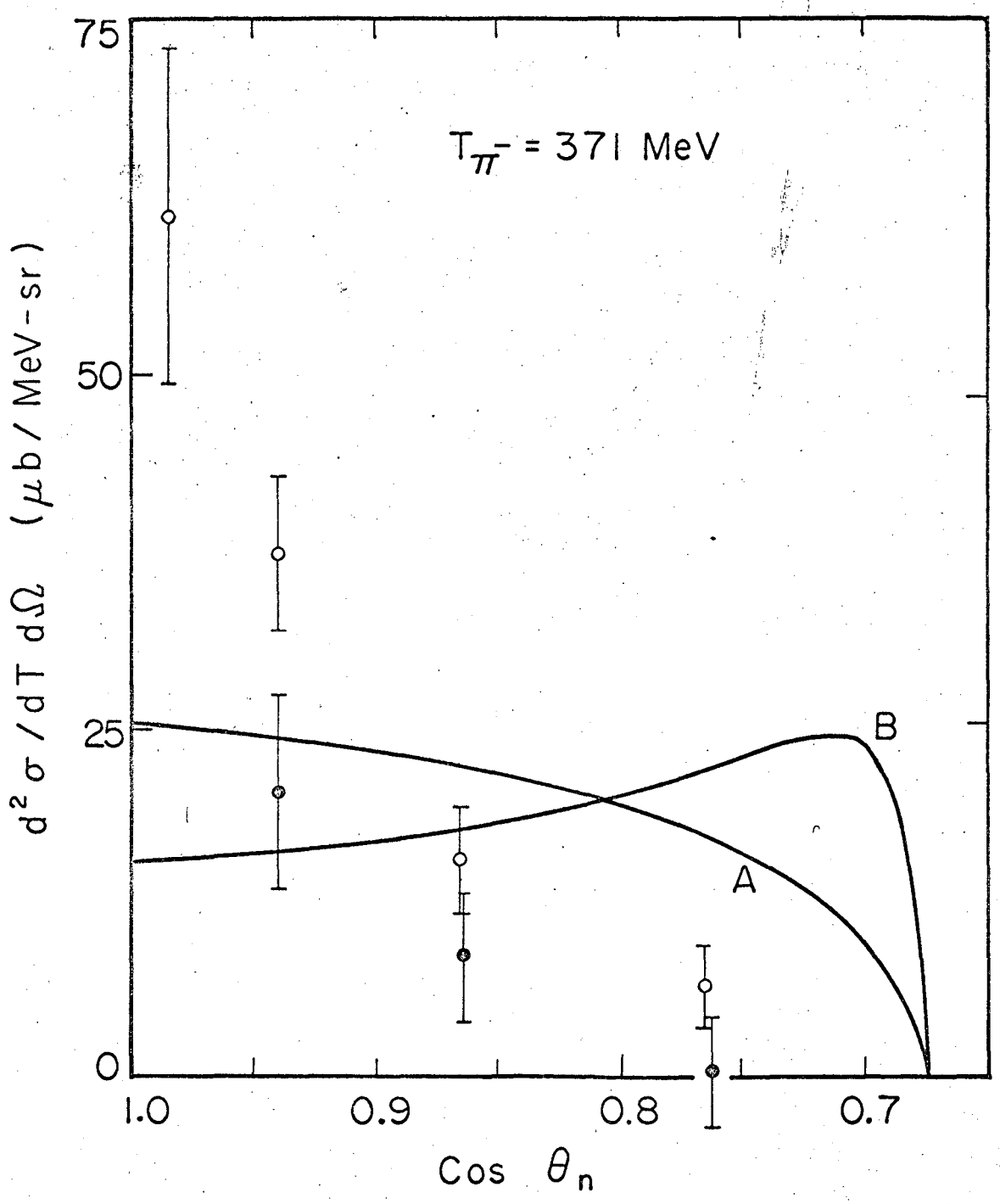

MU-34131

Fig. 7

This report was prepared as an account of Government sponsored work. Neither the United States, nor the Commission, nor any person acting on behalf of the Commission:

A. Makes any warranty or representation, expressed or implied, with respect to the accuracy, completeness, or usefulness of the information contained in this report, or that the use of any information, apparatus, method, or process disclosed in this report may not infringe privately owned rights; or

B. Assumes any liabilities with respect to the use of, or for damages resulting from the use of any information, apparatus, method, or process disclosed in this report.

As used in the above, "person acting on behalf of the Commission" includes any employee or contractor of the Commission, or employee of such contractor, to the extent that such employee or contractor of the Commission, or employee of such contractor prepares, disseminates, or provides access to, any information pursuant to his employment or contract with the Commission, or his employment with such contractor.